Available online at www.sciencedirect.com
ScienceDirect
Journal of Nuclear Materials 363–365 (2007) 377–381
journal of nuclear materials
www.elsevier.com/locate/jnucmat

The effect of the magnetic topology on particle recycling in the ergodic divertor of TEXTOR

M. Lehnen [a,*], S.S. Abdullaev [a], S. Brezinsek [a], K.H. Finken [a], D. Harting [a], M. von Hellermann [b], M.W. Jakubowski [a], R. Jaspers [b], A. Kirschner [a], A. Pospieszczyk [a], D. Reiter [a], U. Samm [a], O. Schmitz [a], G. Sergienko [a], B. Unterberg [a], R. Wolf [a], The TEXTOR Team

[a] *Institut für Plasmaphysik, Forschungszentrum Jülich, Association EURATOM-FZJ, Germany*[1]
[b] *FOM-Rijnhuizen, Association EURATOM-FOM, The Netherlands*[2]

Abstract

The influence of the divertor geometry of the dynamic ergodic divertor (DED) in TEXTOR on particle recycling is discussed. The geometry can be varied by the choice of the base mode, the edge safety factor and the divertor coil current. The divertor volume is split into the upstream and the downstream area. Strong plasma flows in the downstream area, essential for high screening efficiency, are predicted. The source strength of deuterium and carbon in the downstream area is estimated by using the two-dimensional distribution of D_α and CIII emission in front of the target. The results are compared to EMC3 and ERO-code calculations.

PACS: 52.55; 52.25; 52.40

Keywords: Divertor; Edge plasma; Stochastic boundary; Textor

1. Introduction

In this paper, the influence of the DED divertor geometry on the particle recycling behaviour is discussed. Especially the radial extent of the divertor volume with respect to the mean free path of neutrals plays an important role for the control of the recycling in a divertor. Such a control is essential to achieve divertor regimes like high-recycling and improve the impurity screening in the divertor. These properties were first studied in limiter and poloidal divertor machines. More recently these studies were also intensified for helical, island and ergodic divertor geometries [1–4]. The higher complexity of these configurations makes the analysis more challenging.

The ergodic divertor at TEXTOR generates a resonant magnetic perturbation which focuses the

* Corresponding author. Tel.: +49 2461 615102; fax: +49 2461 615452.
E-mail address: m.lehnen@fz-juelich.de (M. Lehnen).
[1] www.fz-juelich.de/ipp.
[2] www.rijnh.nl.

0022-3115/$ - see front matter © 2007 Elsevier B.V. All rights reserved.
doi:10.1016/j.jnucmat.2007.01.125

particle flux on the divertor target plates at the high field side. The magnetic topology is determined by the position of the resonant surfaces (surfaces with low rational safety factor) and the base mode of the divertor coil current distribution [5]. Three base modes have been investigated with poloidal/toroidal mode numbers of $m/n = 3/1$, 6/2 and 12/4. Depending on the base mode, 2, 4 or 8 strike zones appear on the divertor target and neutrals penetrate radially into a complex structure consisting of flux bundles with different connection lengths to the target. An example for $m/n = 6/2$ is given in Fig. 1(a). The target loading pattern is determined by the connection length of the field lines hitting the target. Peak particle and heat fluxes are found where field lines of long connection length hit the target. This is caused by the deep penetration of these field lines up to the last closed flux surface (LCFS). Flux tubes of one poloidal turn length are positioned further away from the LCFS. They are filled by diffusion and can take a substantial part of the particle and heat to the target [6,7].

For the discussion of the particle recycling in the divertor, the plasma flow plays an important role as was shown for example for the ergodic divertor in Tore Supra [8]. Also in poloidal divertors it is the strong flow to the target that facilitates impurity screening. For high screening efficiency, the extent of the so-called 'downstream area' is of importance. This area comprises all field lines, with their shortest distance to the target less than one poloidal turn, e.g. those field lines which do not pass the LFS before they intersect the target (Fig. 1(b)). This definition is in analogy to the downstream area in a poloidal divertor. Within this area, high flow velocities towards the target are expected [6]. Fig. 2 shows an example for $m/n = 6/2$ calculated by the three-dimensional fluid code EMC3 [7,9]. Indicated is the boundary of the downstream area. The Mach number is close to 1 in most of this area, whereas in the upstream area stagnation is seen.

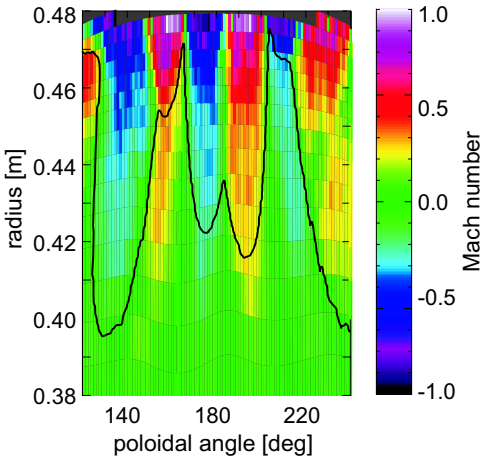

Fig. 2. $m/n = 6/2$ configuration: flow pattern in front of the DED target calculated by EMC3-Eirene. The boundary of the downstream area is indicated by the black line.

2. Source distribution

The aim of this work is to quantify the source distribution for deuterium and carbon. We analyse the radial and poloidal distribution of the D_α and CIII (465 nm) emission with respect to the magnetic

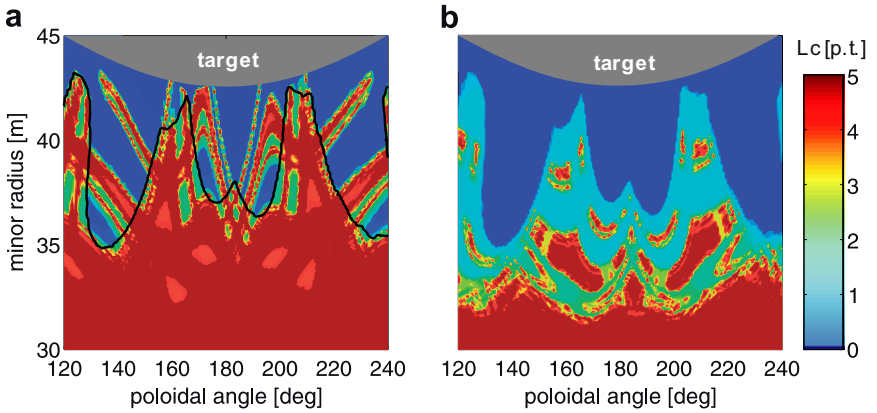

Fig. 1. $m/n = 6/2$ configuration with edge safety factor $q_a = 3.6$. (a) Connection length giving the total length of the field lines in poloidal turns (p.t.) from target to target. Field line tracing is stopped for $L_c > 5$. The black line indicates the boundary of the downstream area. (b) Shortest distance along the field lines from the poloidal plane shown to the target plates. The downstream area (blue) consists of field lines with shortest distance well beneath 0.3 p.t.

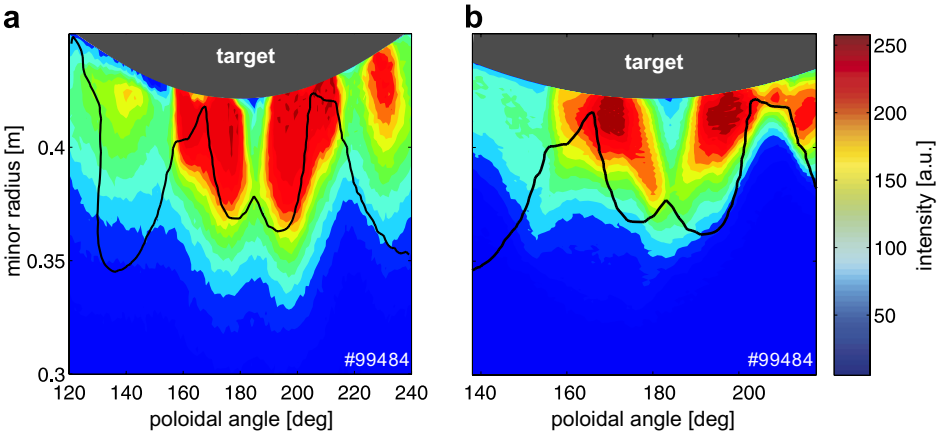

Fig. 3. $m/n = 6/2$ configuration: D_α (a) and CIII (b) emission pattern in front of the DED target.

topology. The ratio between *downstream* sources and total source, Q_{down}/Q_{tot}, has been chosen as a representative parameter describing the recycling pattern. Q_{down} is defined as the line emission integrated over the downstream area, Q_{tot} is the total emission in front of the target.

Fig. 3(a) shows the D_α emission, Fig. 3(b) the CIII emission in front of the target. The black line indicates the boundary of the downstream area. The discharge was heated by neutral beam injection with a total input power of 1.55 MW. The plasma current is $I_P = 315$ kA, the toroidal field $B_t = 1.9$ T, resulting in $q_a = 3.6$. The DED current is 7.5 kA, which is the maximum amplitude for $m/n = 6/2$. The magnetic topology is that shown in Fig. 1. For both species, the main plasma–wall interaction zone is located between 160° and 215°. The CIII pattern is influenced by the plasma parameters which are strongly modulated depending on the field line connection length. The two thin fingers connecting the '*x*-point' at 184° to the target are clearly seen on the emission pattern. This dependence on the plasma parameters is used to identify the predicted magnetic topology at the plasma boundary [10,11].

The extent and structure of the downstream area can be modified by the DED current, the safety factor and the base mode configuration. Fig. 4 shows the ratio Q_{down}/Q_{tot} as a function of the safety factor for the three different base modes. The electron densities vary between 2 and 4×10^{19} m^{-3}. The total heating power is about $P_{tot} = 1.5$ MW (3/1 and 6/2) and $P_{tot} = 0.8(2.4)$ MW (12/4). The DED coil current is varying from 11.5 kA in 12/4 configuration (77% of the nominal value) to 7.5 kA in 6/2 (100%) and 2.0 kA in 3/1 (53%). Restrictions arise

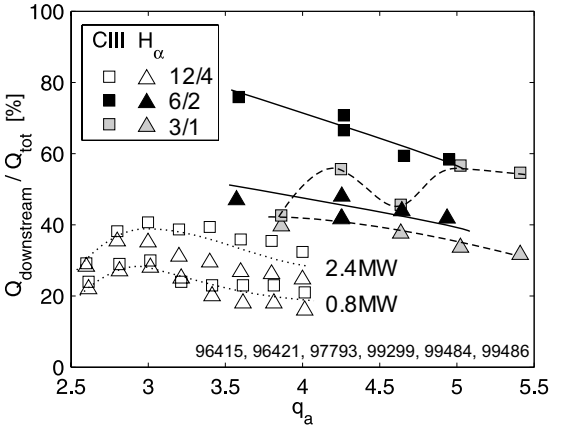

Fig. 4. Fraction of downstream emission for D_α and CIII as function of the edge safety factor. Lines are guide to the eye.

from technical reasons in 12/4 and from the threshold for tearing mode excitation in 3/1 configuration [12]. This excitation threshold limits the accessible q_a range in 3/1 and also in the 6/2 configuration.

The $m/n = 12/4$ base mode operation creates a rather small scale magnetic structure, where flux tubes of different connection length are interwoven in front of the target plates. Most of the neutrals penetrate into regions with field lines which travel more than one poloidal turn until they reach the target. The maximum radial extent of the downstream region is up to 25 mm which is 6% of the plasma minor radius. For both species, D^+ and C^{3+}, we find that Q_{down}/Q_{tot} is at maximum 30% with a peak around the main resonance at $q_a = 3.0$.

The $m/n = 3/1$ base mode operation leads to a more coarse structure where flux bundles of different connection length are well separated and the downstream area is larger compared to the 12/4

base mode. The radial extent of the downstream area for $I_{DED} = 2$ kA is up to 45 mm, which is 10% of the minor radius. In this operation mode up to 45% of the D^+ and even more than 60% of the C^{3+} sources lie inside the downstream area.

The radial extent of the downstream area in the 6/2 base mode is up to 70 mm. Q_{down}/Q_{tot} reaches values of up to 75% for C^{3+} and about 50% for D^+. When the safety factor is decreasing, the radial extent of the downstream area increases and peaks around $q_a = 3.0$. Accordingly Q_{down}/Q_{tot} shows the same dependence.

The source distribution does not only depend on the radial extent of the downstream area and the radial penetration of the neutrals, but also on the detailed topology in radial and poloidal direction. For example, a large safety factor above 6.0 in the case of the 6/2 configuration leads to a topology where most of the particles penetrate into the upstream area. Although the radial extent of the downstream area is still significant, it overlaps strongly with the private flux region with very low source strength.

3. Interpretation by a simple ERO model

In the above analysis, we used the light emission to quantify the source distribution. For D_α emission this is justified, because it reflects the D^+ source. Since the C^{2+} distribution is unknown, the radial source distribution for C^{3+} cannot easily be deduced from the CIII emission. In order to justify Q_{down}/Q_{tot} as a parameter describing the screening efficiency of the ergodic divertor, a simple model was set-up using the ERO code [13]. The model divides the perturbed plasma edge in front of the target into two areas (Fig. 5): (a) the downstream area with Mach number $M = 1$ at the target and a slow decay in radial direction adapted to the EMC3 model results; (b) the upstream area with $M = 0$. Area (a) has a strong modulation of the plasma parameters in poloidal direction with a peak temperature of $T_i = T_e = 50$ eV and a peak density of $n_e = 5 \times 10^{19}$ m^{-3} at the position of the strike point. The e-folding length of the plasma parameters is assumed to be 20 mm towards the private flux zone (area around $\theta = 180°$) and 70 mm towards the DED-SOL. These values are adapted from target probe measurements [10]. The plasma parameters increase linearly towards the boundary of the area (b), where the plasma parameters are kept constant along the poloidal direction and increase in radial direction to approximate the experimental values.

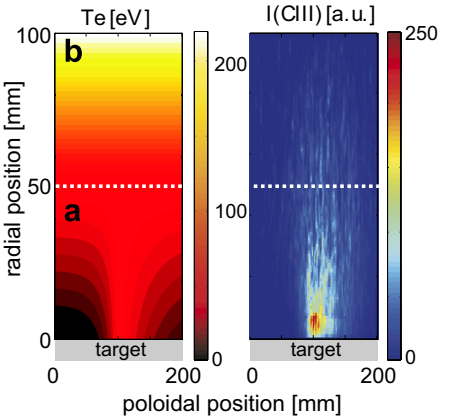

Fig. 5. ERO model: temperature distribution in the model volume (left). The temperature in the strike point and at the boundary to the upstream area is 50 eV. The density has the same distribution. Shown is an example for $\delta_{down} = 50$ mm CIII emission as calculated by ERO (right).

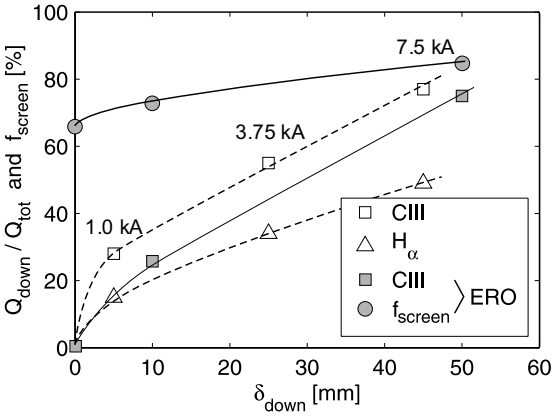

Fig. 6. Fraction of downstream emission for D_α and CIII as function of the width of the downstream region for the $m/n = 6/2$ configuration. The screening factor f_{screen} and Q_{down}/Q_{tot} calculated by the simple ERO model is added. Lines are guide to the eye.

Fig. 6 shows the relative downstream emission as a function of the width of the downstream area δ_{down} for the base mode $m/n = 6/2$. Increasing the DED coil current leads to a broadening of that area. Accordingly Q_{down}/Q_{tot} increases. This dependence is well reproduced by the simple model. The screening efficiency is described in the model by the factor f_{screen}, which is the ratio between carbon atoms/ions redeposited on the target and the overall carbon source at the wall. This factor is increased from $\delta_{down} = 0$–50 mm by about 30%. It has to be noted that the simplified magnetic geometry (all field lines

in the volume are connected to the target) leads to a statistical offset of $f_{screen} = 50\%$ at $\delta_{down} = 0$.

4. Conclusions

The ergodic divertor at TEXTOR can provide a sufficiently broad divertor volume to screen impurities from the confined plasma. However, no strong effect on the C^{6+} concentration measured by CXRS for $r/a < 0.65$ is seen. The absolute value of the impurity concentration in the plasma center varies at maximum by 30%. In most cases an increase of the carbon content in the core is seen, which might be caused by increased impurity fluxes at e.g. hot spots on the divertor tiles or particle transport changes. A reduction of the core contamination is seen in discharges with reversed neutral beam injection, which might be related to confinement changes provoked by the DED. These effects are not yet understood and have to be investigated further.

In contrast to limiter operation, the high-recycling regime is easily accessed in poloidal divertor machines, because of the localised ionisation in front of the target plates. For the calculation of the ionisation fraction in the DED downstream area, the integration in poloidal and radial direction is essential, because of the strongly varying width of this area. The comparison between ionisation length (in this case 20–40 mm) and averaged extent of the downstream area ($\delta_{down} = 50$ mm) might overestimate the screening efficiency. A maximum ionisation fraction inside the DED downstream area of about 50% is found for the 6/2 configuration. This is less than estimated for poloidal divertors [14] or island divertors (>75%) [15]. Accordingly, a high-recycling regime as it was found in the ergodic divertor of Tore Supra [3] was not yet seen in this configuration. This might be related to the divertor geometry and a larger extent of the perturbed volume; the plasma parameters in the divertor are of comparable magnitude for TEXTOR and Tore Supra. However, the divertor screening of the DED might be further increased with higher heating power and densities.

The simple ERO model gives a rough estimate for the screening efficiency of the DED. It does not account for the three-dimensional structure of the plasma parameters in the perturbed boundary layer. For a more detailed analysis, the code EMC3–EIRENE including carbon transport has to be used. Moreover, modelling with the ERO code using a background plasma produced by EMC3 will give more insight into the carbon source distribution, which is needed to quantify the impurity screening.

Acknowledgement

This work has been partially supported by the Sonderforschungsbereich (SFB) 591 of the Deutsche Forschungsgemeinschaft (DFG).

References

[1] R. König et al., Plasma Phys. Control. Fus. 44 (2002) 2365.
[2] T. Morisaki et al., J. Nucl. Mater. 337–339 (2005) 154.
[3] J. Gunn et al., Plasma Phys. Control. Fus. 41 (1999) B243.
[4] Ph. Ghendrih et al., Nucl. Fus. 42 (2002) 1221.
[5] K.H. Finken et al., The structure of magnetic field in the TEXTOR-DED, Schriften des Forschungszentrum Jülich, Energy Technology 45, 2005. ISSN 1433-5522.
[6] Th. Eich, D. Reiser, K.H. Finken, J. Nucl. Mater. 290–293 (2001) 849.
[7] O. Schmitz et al., J. Nucl. Mater., these Proceedings, doi:10.1016/j.jnucmat.2007.01.067.
[8] R. Giannella et al., Plasma Phys. Control. Fus. 43 (2001) 271.
[9] M. Kobayashi et al., Nucl. Fus. 44 (2004) S64.
[10] M. Lehnen et al., Plasma Phys. Control. Fus. 47 (2005) B237.
[11] M.W. Jakubowski, O. Schmitz, et al., PRL 96, 035004.
[12] H.R. Koslowski et al., Nucl. Fus. 46 (2006) L1–L5.
[13] A. Kirschner, V. Philipps, U. Kögler, J. Winter, Nucl. Fus. 40 (2000) 989.
[14] C.S. Pitcher, P.C. Stangeby, Plasma Phys. Control. Fus. 39 (1997) 779.
[15] Y. Feng et al., J. Nucl. Mater. 313–316 (2003) 857.